Cellular pathophysiological consequences of BCS1L mutations in mitochondrial complex III enzyme deficiency

Maria Moran, Lorena Marín Buera, Maria Carmen Gil, Henry Rivera, Alberto Blazquez, Sara Seneca, Maria Vazquez Lopez, Joaquin Arenas, Miguel A Martin, Cristina Ugalde

Human Mutation

Cellular pathophysiological consequences of BCS1L mutations in mitochondrial complex III enzyme deficiency

Journal:	*Human Mutation*
Manuscript ID:	humu-2010-0090.R1
Wiley - Manuscript type:	Research Article
Date Submitted by the Author:	23-Apr-2010
Complete List of Authors:	Moran, Maria; Hospital Universitario 12 de Octubre, Centro de Investigacion Marín Buera, Lorena; Hospital Universitario 12 de Octubre, Centro de Investigacion Gil, Maria Carmen; Hospital Universitario 12 de Octubre, Centro de Investigacion Rivera, Henry; Hospital Universitario 12 de Octubre, Centro de Investigacion Blazquez, Alberto; Hospital Universitario 12 de Octubre, Centro de Investigacion Seneca, Sara; AZ-VUB, Center of Medical Genetics Vazquez Lopez, Maria; Hospital General Universitario Gregorio Marañón, Sección de Neuropediatría Arenas, Joaquin; Hospital Universitario 12 de Octubre, Centro de Investigación; Hospital Universitario 12 de Octubre, Centro de Investigacion Martin, Miguel; Hospital Universitario 12 de Octubre, Centro de Investigación; Hospital Universitario 12 de Octubre, Centro de Investigacion Ugalde, Cristina; Hospital Universitario 12 de Octubre, Centro de Investigacion
Key Words:	Mitochondria, Respiratory chain , Complex III deficiency, BCS1L mutations

Cellular pathophysiological consequences of *BCS1L* mutations in mitochondrial complex III enzyme deficiency

María Morán,[1,2,*] Lorena Marín-Buera,[1,2,*] M. Carmen Gil-Borlado,[1,2] Henry Rivera,[1,2] Alberto Blázquez,[1,2] Sara Seneca,[3] María Vázquez-López,[4] Joaquín Arenas,[1,2] Miguel A. Martín,[1,2] and Cristina Ugalde[1,2]

* These authors equally contributed to this work

[1]Centro de Investigación, Hospital Universitario 12 de Octubre, Madrid, Spain; [2]Centro de Investigación Biomédica en Red de Enfermedades Raras (CIBERER), U723, Spain; [3]Center of Medical Genetics, AZ-VUB, Brussels, Belgium; and [4]Sección de Neuropediatría, Hospital General Universitario Gregorio Marañón, Madrid, Spain.

Corresponding author: Dr. Cristina Ugalde, Centro de Investigación, Hospital Universitario 12 de Octubre. Avda. de Córdoba s/n. 28041 Madrid. Phone: +34 91 390 8763, FAX: +34 91 390 8544, e-mail: cugalde@h12o.es

Abbreviated title: Role of mutated *BCS1L* in complex III deficiency

ABSTRACT

Mutations in BCS1L, an assembly factor that facilitates the insertion of the catalytic Rieske Iron-Sulphur subunit into respiratory chain complex III, result in a wide variety of clinical phenotypes that range from the relatively mild Björnstad syndrome, to the severe GRACILE syndrome. To better understand the pathophysiological consequences of such mutations, we studied fibroblasts from six complex III-deficient patients harbouring mutations in the *BCS1L* gene. Cells from patients with the most severe clinical phenotypes exhibited slow growth rates in glucose medium, variable combined enzyme deficiencies and assembly defects of respiratory chain complexes I, III and IV, increased H_2O_2 levels, unbalanced expression of the cellular antioxidant defences, and apoptotic cell death induction. Besides, all patients showed cytosolic accumulation of the BCS1L protein, suggestive of an impaired mitochondrial import, assembly or stability defects of the BCS1L complex, fragmentation of the mitochondrial networks, and decreased MFN2 protein levels. The observed structural alterations were independent of the respiratory chain function and ROS production. Our results provide new insights into the role of pathogenic *BCS1L* mutations in mitochondrial function and dynamics.

KEYWORDS: Mitochondria; respiratory chain complex III deficiency; *BCS1L* mutations.

INTRODUCTION

Mitochondrial respiratory chain complex III (CIII, ubiquinol-cytochrome c oxidoreductase or cytochrome bc1 complex, E.C.1.10.2.2) catalyzes the transfer of electrons from reduced coenzyme Q to cytochrome c with a concomitant translocation of protons across the inner membrane (Baum et al., 1967). The purified bovine complex is a ~450 kDa symmetric homodimer (Iwata 1998; Xia et al., 1997). Each monomer is composed of eight structural subunits, and three catalytic subunits: cytochrome b, the only subunit encoded in the mitochondrial genome, cytochrome c1, and the Rieske Iron-Sulphur Protein (RISP).

Mitochondrial complex III enzyme deficiency (MIM #124000) is a relatively infrequent diagnosed defect of the oxidative phosphorylation (OXPHOS) system (Benit et al., 2009). The vast majority of nuclear mutations leading to complex III deficiency have been reported in the *BCS1L* gene (MIM #603647), which encodes a mitochondrial inner membrane protein necessary for the correct biogenesis of respiratory chain complex III (Cruciat et al., 1999; Fernandez-Vizarra et al., 2007; Fernandez-Vizarra et al., 2009; Nobrega et al., 1992). *BCS1L* mutations lead to three main clinical phenotypes (Ramos-Arroyo et al., 2009): i) Björnstad syndrome (MIM #262000), an autosomal recessive disorder characterized by sensorineural hearing loss and *pili torti* (Hinson et al., 2007); ii) GRACILE syndrome (MIM #603358), a Finnish-heritage disease caused by the homozygous p.S78G mutation (Fellman 2002; Visapaa et al., 2002), which is characterized by fetal growth retardation, aminoaciduria, cholestasis, iron overload, lactic acidosis, and early death; and iii) complex III deficiency in neonates or infants presenting with encephalopathy, alone or in combination with visceral involvement (Blazquez et al., 2009; de Lonlay et al., 2001; De Meirleir et al., 2003; Fernandez-Vizarra et al., 2007; Gil-Borlado et al., 2009).

Human BCS1L protein consists of 419 aminoacids, and shares functional homology and 50% identity with yeast Bcs1p (Nobrega et al., 1992; Petruzzella et al., 1998). In yeast, Bcs1p acts as an ATP-dependent chaperone, maintaining pre-complex III in a competent state for the subsequent assembly of the Rieske and Qcr10 subunits (Cruciat et al., 1999). The absence of Bcs1p prevents the assembly of Rieske within complex III and leads to a complete respiratory deficiency. Bcs1p spans three different domains: i) the N-terminal domain comprises aminoacid residues 1 to 126, which contain all the required information for the mitochondrial targeting and sorting of the protein (Folsch et al., 1996; Petruzzella et al., 1998); ii) a Bcs1p-specific domain contains aminoacid residues that are important for Bcs1p activity and stability (Nouet et al., 2009); and iii) the C-terminal region contains a ~200 aminoacids domain that encompasses two motifs corresponding to nucleotide binding sites, a characteristic feature of the AAA (for ATPases associated with various cellular activities) protein superfamily (Frickey and Lupas, 2004).

Pathogenic mutations have been described in the three different domains of human BCS1L, although the pathophysiological mechanisms that contribute to the clinical manifestations of the disease remain poorly understood. In some *BCS1L*-mutated patients presenting with Björnstad syndrome or complex III deficiency, an assembly defect of the RISP subunit led to a mitochondrial complex III enzyme defect (Blazquez et al., 2009; Fernandez-Vizarra et al., 2007; Gil-Borlado et al., 2009; Hinson et al., 2007). However, in patients presenting with the characteristic *BCS1L* mutation c.232A>G (p.S78G) leading to GRACILE syndrome, complex III activity was essentially normal despite low BCS1L levels (Fellman et al., 2008). Iron overload has been reported in some patients with *BCS1L* mutations leading to GRACILE syndrome or complex III deficiency, but not Björnstad Syndrome, suggesting a second hypothetic role for BCS1L in iron metabolism (De Meirleir et al., 2003; Visapaa et al., 2002). It

has also been proposed that the pathophysiology of the *BCS1L* mutations might be regulated by reactive oxygen species (ROS) production in a mutation and disease-dependent manner (Hinson et al., 2007). In human cells, *BCS1L* knockdown caused the disassembly of the mitochondrial supercomplexes, and led to morphological alterations of the mitochondrial network (Tamai et al., 2008). Besides, it caused the down regulation of LETM1, a mitochondrial Ca^{2+}/H^{+} antiporter that is implicated in the human Wolf-Hirschhorn syndrome (Jiang et al., 2009; Tamai et al., 2008).

In order to unveil the cell biological consequences of *BCS1L* defects, we have performed a comparative series of cellular and biochemical studies in skin fibroblasts from six complex III-deficient patients harbouring mutations in the *BCS1L* gene. Our results establish a correlation between specific cellular pathophysiological effects of such mutations and the severity of the clinical manifestations of the disease, and provide new insights into the role of BCS1L in mitochondrial function and dynamics.

PATIENTS, MATERIALS AND METHODS

Patients

Patient 1 was an 11 days old female, born to parents who were first cousins, whose body weight, height and head circumference were below 3rd percentile. Clinical examination showed hypotonia, weak reflexes, and mild hepatomegaly. Blood chemistry revealed marked lactic acidosis (6.8 mmol/L, normal <2.0), elevation of liver enzymes and alanine levels, decreased serum albumin, elevated ferritin levels, and decreased total iron binding capacity and transferrin levels. Organic acids analysis in urine displayed prominent lactic aciduria, and mild increase in 2-OH butyric, 3-OH butyric, fumaric, succinic, and 4-OH phenyl-lactic acid levels. There was also generalized aminoaciduria, glucosuria and hyperphosphaturia consistent with renal Fanconi syndrome. A mitochondrial disease was suspected, and a treatment with coenzyme Q, carnitine, vitamins and cofactors was initiated that failed to correct acidosis. The *BCS1L* gene was sequenced based on some key described clinical features, such as lactic acidosis, hepatopathy, iron overload, and tubulopathy, together with neurological signs, which are often found in patients with mutations in this gene (de Lonlay et al., 2001; De Meirleir et al., 2003); therefore; no muscle biopsy was performed. Peritoneal dialysis was unsuccessful because of the presence of severe peritonitis, which was treated with intravenous antibiotics. Although enteral nutrition led to weight gain and sodium bicarbonate therapy managed eventually to control the metabolic acidosis, she died at 7 months of age by a *Pseudomonas* sepsis.

Patient 5, a girl of 19 months of age born to non-consanguineous parents, presented with fever, seizures, progressive deterioration of consciousness, and respiratory dysfunction. Neurological examination showed hypertonia, hyperintense deep tendon reflexes, and an extensor response in the plantar reflex. Laboratory data showed a dramatic increase in the serum levels of AST and ALT (>6000 IU/L), and

increased serum lactate (2.9 mmol/L, normal <2.0). Brain CT scanning showed bilateral hypodensities in brainstem, thalamus, and basal ganglia. Brain MRI displayed supra and infratentorial symmetric bilateral white matter lesions, as well as bilateral T2-weighted hyperintense signals in the thalamus. Clinical examination at age 5 years revealed hypertonia with hypereflexia and spasticity in the upper and lower limbs.

Patients 2, 3, 4 and 6 were reported before (Blazquez et al., 2009; De Meirleir et al., 2003; Gil-Borlado et al., 2009). A summary of clinical, genetic, and biochemical data from the six complex III-deficient patients is shown in Table 1.

Enzyme activities of mitochondrial respiratory chain complexes

Mitochondrial respiratory chain enzyme activities (Table 2) were performed in cultured skin fibroblasts according to established methods (Blazquez et al., 2009).

Genomic DNA sequence analysis

Total DNA was extracted from fibroblasts by standard methods. Sequencing of the mitochondrial *MT-CYB* gene (MIM #516020), which encodes the complex III cytochrome b subunit, excluded mutations in this gene. Overlapping fragments of the entire *BCS1L* genomic region, which included all exons, introns, and the 5' and 3' UTR regions, were sequenced on an ABI Prism System 3130xL Genetic Analyzer (Applied Biosystems), and compared with the GenBank reference sequence for the *BCS1L* gene (NG_008018.1). The mutations were confirmed by PCR-RFLP analyses, and four hundred alleles of healthy ethnically-matched controls were screened for the mutations.

Fibroblast cultures and cell growth analysis

Cultured skin fibroblasts from patients and controls were plated in 4.5 g/l glucose-containing Dulbecco´s modified Eagle´s Medium (DMEM) (Invitrogen) supplemented with 10% fetal bovine serum (FBS) and 100 IU/ml penicillin and 100 IU/ml streptomycin. Mycoplasma testing was performed by DAPI staining and

epifluorescence microscopy in fibroblasts, which yielded negative results. Cells were balanced for passage number. Multiple series of P10 plates were seeded each with a constant number of cells ($5x10^5$) and cell growth was assessed in normal glucose medium. Triplicate plates were trypsinized and counted daily for 4 days.

SDS-PAGE analysis

Whole cell homogenates were prepared by resuspending $2x10^6$ cells in 125 µl PBS containing 2% (w/v) n-dodecyl ß-D-maltoside. Following 15 min incubation on ice, homogenates were centrifuged (30 min, 12000 g, 4°C). The supernatant was mixed with an equal volume of Tricine sample buffer (Biorad) containing 2% (v/v) 2-mercaptoethanol. The mixture was kept at room temperature for 60 min. Proteins were separated on 10 % polyacrylamide gels and transferred to PROTRAN® nitrocellulose membranes (Whatman GmbH).

Cellular fractionation

Approximately $4x10^6$ fibroblasts were harvested, washed in PBS, resuspended in an appropriate isotonic buffer (0.25 M sucrose, 10 mM Tris-HCl pH 7.8, 0.2 mM EDTA, and 0.1 mM PMSF) and homogenized using ReadyPrep™ Minigrinders (Biorad). Unbroken cells and nuclei were pelleted by centrifugation at 1000 g for 10 min. Supernatants were centrifuged at 10000 g for 25 min. The resulting supernatant was isolated as the cytoplasmic fraction and subject to Western-blot analysis.

Assessment of assembly and/or stability of mitochondrial OXPHOS complexes

Two-dimensional blue native gel electrophoresis (2D-BN/SDS-PAGE) and mitochondrial complex I *in gel* activity assay were performed with digitonin-enriched mitochondrial fractions from the six patients´ fibroblasts and up to five different control fibroblasts, as described elsewhere (Nijtmans et al., 2002).

Antibodies

Western-blot analyses were performed with antibodies raised against the following proteins: polyclonal BCS1L (ProteinTech Group); monoclonal BCS1L (Abnova); mitochondrial complex I NDUFA9 and NDUFS3 subunits, complex II SDHA subunit, complex III Rieske Iron-Sulphur protein (RISP) and core 2 protein, and complex IV COX2 and COX5A subunits (Molecular Probes); DRP1 and OPA1 (BD Biosciences); MFN2 (Abnova); gluthatione peroxidase (GPx, Assay Designs); gluthatione reductase (GR, Abcam); MnSOD, catalase (CAT), and β-actin (Sigma). Peroxidase-conjugated anti-mouse or anti-rabbit IgGs (Molecular Probes) were used as secondary antibodies. The signal was detected with ECL® plus (Amersham Biosciences). Band densities were evaluated by densitometric scanning (Image J).

Indirect Immunofluorescence

Cells were fixed with 4% paraformaldehyde for 15 min and permeabilized for 15 min with 0.1% Triton X-100. Cells were incubated in blocking buffer containing 10% goat serum for 1h at room temperature. The mouse monoclonal anti-complex V α subunit (MitoSciences) was used as a primary antibody. Texas Red-conjugated anti-mouse (MitoSciences) was used as a secondary antibody. After appropriate rinsing, cover slips were mounted in ProLong Gold antifade reagent (Molecular Probes) on glass slides, and cells were viewed with a Zeiss LSM 510 Meta confocal microscope and a 63x planapochromat objective.

Analysis of intracellular ROS in live cells by confocal microscopy

Cultured skin fibroblasts grown on cover slips were loaded with 5 μM 2', 7'-dichlorofluorescein diacetate (DCF-DA, Sigma) for 20 min in the dark in a CO_2 incubator. After loading, the dye was removed and cells were washed twice with PBS before image collection with a Zeiss LSM 510 Meta confocal microscope. The image collection was carried out with a 20x lens plus a 2x digital zoom using the 488 nm excitation laser line.

Measurement of intracellular ROS production by Flow Cytometry

Cells were grown until 65% confluence, trypsinized and resuspended in fresh medium. Cell suspensions were incubated for 30 min at 37 ºC in a CO_2 incubator with 5 µM DCF-DA. To measure the intracellular H_2O_2 levels, the DCF-DA fluorescence was excited by a 15 mW laser tuned to 488 nm and the emitted fluorescence was measured in a FACscan Becton Dickinson flow cytometer. Data acquisition and analysis was performed using the Cell Quest program (Becton Dickinson).

Cell death quantification

Apoptotic cells were quantified in skin fibroblasts with the In Situ Cell Death Detection kit, Fluorescein (Boehringer Mannheim) – based on the TUNEL method – and by Cell Death Detection ELISA^{PLUS} assay (Roche), used to quantify DNA fragmentation in fibroblast cells undergoing apoptosis, according to the manufacturers´ protocols.

Data Analysis

All determinations were performed at least in triplicate. Mitochondrial morphology was determined as follows: the proportion of cells with essentially elongated filamentous mitochondria (% of elongated), with an intermediate mitochondrial morphology (% of intermediate), or with only punctuate mitochondria (% of punctuate) was determined in five different controls and each of the patients´ fibroblast cell lines by three independent examiners (Guillery et al., 2008). To measure mitochondrial diameter (width), the Image J software was used after setting the scale in the images according to the objective employed to obtain the photographs; results were presented as mean (±SD) values of 200 determinations for each cell line (Moran et al., 2010). One-way ANOVA analysis was used for statistics. When a significant *P*-value was obtained, the Scheffé test was employed *post hoc* to determine differences between groups. A level of $P<0.05$ was selected to indicate statistical significance.

RESULTS

Clinical, genetic and biochemical features of the *BCS1L* patients.

We studied six patients, in five of whom (P2-P6) a major respiratory chain complex III defect was previously identified either in muscle homogenates or fibroblasts (Blazquez et al., 2009; De Meirleir et al., 2003; Gil-Borlado et al., 2009). We first excluded mutations in the mitochondrial *MT-CYB* gene, which encodes the complex III cytochrome b subunit.

Sequencing of the entire *BCS1L* genomic sequence and PCR-RFLP analyses in fibroblasts DNA revealed the presence of mutations in all patients (Figure 1A, Table 1). Patient P1 was homozygous for the reported c.296C>T (p.P99L) mutation (de Lonlay et al., 2001), and patients P2 and P3, who were siblings, were compound heterozygous for the c.133C>T (p.R45C) and c.166C>T (p.R56X) mutations (De Meirleir et al., 2003). These three patients, who died before 8 months of age, displayed all the classic symptoms of *BCS1L*-associated complex III deficiency except for signs of encephalopathy, which were only present in patients P1 and P2. They presented with lactic acidosis, hepatopathy, hypotonia, and iron overload, usually associated with GRACILE syndrome. In addition, patients P1 and P2 had renal dysfunction, and patients P2 and P3 exhibited hypoglycemia. Patient P1 showed a combined defect of respiratory chain complexes I, III, and IV in fibroblasts, and patient P2 showed a combined defect of respiratory chain complexes I and III (Table 2). Due to the poor growth of the fibroblasts from patient P3, we could not get enough amount of sample for the spectrophotometric activity measurements. A respiratory chain complex III deficiency was previously shown in fibroblasts from this patient (De Meirleir et al., 2003), although it could not be determined whether it was a single or a combined enzyme defect because complex I activity was not measured. Patient P4 was compound

heterozygous for the mutations c.166C>T (p.R56X), g.1181A>G and g.1164C>G (Gil-Borlado et al., 2009), and showed a combined defect of respiratory chain complexes III and IV in fibroblasts (Table 2). Patient P6 was homozygous for the c.148A>T (p.T50A) mutation, and had a single complex III defect in fibroblasts (Blazquez et al., 2009). Both patients presented with hepatopathy, lactic acidosis, and hypoglycemia, but patient P4 presented a worse disease progression leading to death before 1 year of age. Patient P5 constitutes a particular case. This patient presented with lactic acidosis, hepatopathy, encephalopathy, and a single complex III defect in muscle, which was not observed in fibroblasts (Table 2). She harboured the previously reported p.R184C mutation in one allele (Fernandez-Vizarra et al., 2007; Hinson et al., 2007), and also carried a homozygous g.1892A>G genetic variant that, like the previously reported g.1433T>A mutation (Visapaa et al., 2002), lies within an intronic region in the 5' upstream regulatory sequence of *BCS1L*. Due to the lack of muscle sample, reverse transcriptase PCR analysis of *BCS1L* cDNA was performed in fibroblasts from patient P5, which excluded missplicing due to a putative deep intronic mutation missed by standard sequencing (data not shown). Similarly, real-time PCR analysis excluded alterations in *BCS1L* transcript levels (data not shown). These results suggest that the g.1892A>G polymorphism is not pathogenic. No other nucleotide variations were found after sequencing the whole *BCS1L* genomic region, suggesting that the p.R184C change might behave as a manifesting heterozygous mutation. In support of this observation, the p.R184C mutation has been always reported as compound heterozygous in several patients presenting with either complex III deficiency or Björnstad syndrome (Fernandez-Vizarra et al., 2007; Hinson et al., 2007). Neurological signs were observed in patients P1, P2, P5 and P6, which could be related to the possible morphogenetic role of BCS1L in the formation of neural tube structures (Kotarsky et al., 2007). In patient

P3 these neurological alterations were not apparent, maybe due to the fact that she died soon after birth (Table 1).

Growth capabilities of *BCS1L* mutated fibroblasts.

In normal glucose medium, growth rates were reduced in all patients' fibroblasts compared to controls, and revealed substantial differences among the mutant cell lines investigated (Figure 1B). Fibroblasts from patient P5 showed a moderate growth rate, whereas those from patient P6 showed a slightly less efficient growth capacity. Fibroblasts from patients P1, P2, and P4 exhibited similar growth rates, slower than those from patients P5 and P6. Cell growth was severely compromised in fibroblasts from patient P3, which presented the slowest cell growth rate.

Effect of the *BCS1L* mutations on the expression, subcellular location and assembly of the BCS1L protein.

To examine the steady-state expression levels of the BCS1L protein and respiratory chain subunits in mutant fibroblasts, whole cell lysates were analyzed by dodecylsulfate-polyacrylamide gel electrophoresis (SDS–PAGE) followed by Western-blot. As observed in Figure 2A, BCS1L expression was similar in patients´ and control fibroblasts. However, the levels of the complex III Rieske Iron-Sulphur protein (RISP) showed prominent differences among patients. A ~40-60 % reduction in RISP expression was observed in patients P1, P2 and P3, while in the remainder three patients protein levels were similar to controls. In agreement with previous observations this reduction was specific, as the amount of other complex III subunits (such as Core2) was comparable between patients and controls (Fernandez-Vizarra et al., 2007; Hinson et al., 2007). The steady-state levels of other respiratory chain subunits, such as complex I NDUFA9, complex IV COX5A or complex II SDHA, were comparable between patients and controls.

In our patients, most mutations were located within the mitochondrial targeting and sorting domains of the BCS1L protein (Figure 1A). To investigate the cellular localization of BCS1L, we performed subcellular fractionations of control and mutant fibroblasts, and the cytoplasmic fractions were subject to Western-blot analysis. As observed in Figure 2B, BCS1L was absent in the cytosolic fractions of control fibroblasts, while it accumulated at high levels in the cytoplasmic fractions from patients P2, P3, P4, and P6, and mildly accumulated in patients P1 and P5. Mitochondrial contamination was excluded with an antibody against the complex IV COX2 subunit. These results suggest that the mitochondrial import of BCS1L might be hampered in all patients.

Next, mitochondrial-enriched fractions were separated by blue native gel electrophoresis (BN-PAGE) to evaluate both the intramitochondrial BCS1L steady-state levels, and the physical state of the BCS1L complex in mutant fibroblasts (Figure 2C). As expected, Western-blot analysis with an antibody against the BCS1L protein showed a marked reduction in the amount of the ~400 kDa BCS1L complex in fibroblasts from patients P2, P3, P4, and P6 relative to controls, and normal levels in patients P1 and P5. Additionally, a substantial accumulation of two lower subcomplexes of ~200 kDa and ~100 kDa was observed in patients P1-P5. These signals could correspond to either BCS1L complex assembly intermediates or breakdown products that accumulate due to possible structural alterations in the mutated BCS1L proteins. These results were confirmed by two-dimensional blue native gel electrophoresis (2D-BN/SDS-PAGE) of the mitochondrial native complexes (Supplemental Figure S1). Controls predominantly showed the fully-assembled BCS1L complex (~400 kDa) with absence of lower subcomplexes (Supplemental Figure S1, upper panel), whereas all patients' samples showed either reduced levels of the fully-assembled BCS1L complex or an accumulation of lower molecular weight subcomplexes. These results indicate that the

assembly and/or stability of the mitochondrial BCS1L complex are also severely affected in all patients.

Physical state of the mitochondrial respiratory chain complexes in *BCS1L* mutated fibroblasts.

To evaluate the physical state of the respiratory chain complexes in our *BCS1L* mutant fibroblasts, a duplicate BN-PAGE gel was blotted and further analyzed by Western-blot using antibodies raised against different OXPHOS subunits. When an antibody against the complex III RISP subunit was used, decreased steady-state levels of the ~450 kDa complex III dimer were found in fibroblasts from patients P1-P3 (Figure 2D, third panel). Additionally, the RISP subunit accumulated in a ~300 kDa subcomplex in patients P1 and P4. This accumulation product was absent in the control samples, and did not co-localize with any of the BCS1L complexes. Complex III expression levels were normal in patients P5 and P6. Therefore, our results indicate a complex III assembly or stability defect in patients P1-P4, which correlated with the complex III enzyme activities shown in Table 2. Incubation with an antibody that recognizes the complex I NDUFS3 subunit (Figure 2D, second panel) revealed decreased steady-state levels of fully-assembled complex I in patients P1, P2 and P3, but normal complex I levels in the remaining patients. In agreement with the spectrophotometric respiratory chain enzyme measurements in Table 2, a complex I *in-gel* activity (IGA) assay (Figure 2D, upper panel) also showed low complex I activities in patients P1, P2 and P3 compared to controls. Patient P5 also displayed a slight reduction in complex I activity. This reduction neither correlated with the previous biochemical activity measurements nor with the normal expression levels of complex I, raising doubts about its functional significance. Patients P4 and P6 showed normal complex I enzyme activities. Western blot analysis using an antibody against complex

IV COX5A subunit revealed slightly decreased steady-state levels of this complex in patients P1 and P4 (Figure 2D, fourth panel), which also correlated with the corresponding cytochrome c oxidase activities. Finally, the levels of respiratory chain complex II were comparable between all patients and controls (Figure 2D, fifth panel). The signals from the blots were quantified, and the complex I/complex II, complex III/complex II, and complex IV/complex II ratios were used as numerical values for the expression levels of fully-assembled complexes I, III and IV, respectively (Supplemental Figure S2). This whole data set confirmed a combined assembly/stability defect of the respiratory chain in patients P1 to P4.

Structural alterations of the mitochondrial network.

To assess the mitochondrial morphology of our *BCS1L* mutant fibroblasts, we performed confocal microscopy studies by immunofluorescence using an antibody against the ATP synthase (complex V) α-subunit (Figure 3A). As expected, control fibroblasts displayed a majority of highly elongated branched mitochondrial filaments, and the presence of some shorter tubules in a minority of control cells (Benard and Rossignol, 2008; Guillery et al., 2008). Conversely, all patients´ fibroblasts showed abnormal mitochondrial morphologies in glucose medium, with predominantly fragmented phenotypes along with the accumulation of perinuclear short entangled tubules, punctuate mitochondria and ring structures (Figures 3B and 3C). The most severe structural alterations were observed in fibroblasts from patients P2 and P3, which in general displayed a punctuate or an intermediate mitochondrial morphology with many short mitochondrial tubules, and a low number of elongated branched mitochondria (Figure 3C). The mitochondrial transversal section (width) was also measured in our control and mutant fibroblasts, since this is the most constant dimension of the organelle, and variations in this parameter reflect alterations of the mitochondrial morphology (Moran et al., 2010; Santamaria et al., 2006). As observed in

Figure 3D, all patients´ fibroblasts exhibited a significant increase in mitochondrial diameter (one-way ANOVA main effect: $P<0.001$), supporting our previous observations.

We also analyzed the expression of proteins that regulate the fusion-fission events by Western-blot using whole cell lysates from control and *BCS1L* mutant fibroblasts (Figure 4A). The steady-state levels of the DRP1 and OPA1 proteins, involved in mitochondrial fission and fusion, respectively, were comparable between mutant and control fibroblasts. Mild decreased expression levels of the MFN2 fusion protein were found in all mutants. The signals corresponding to MFN2 expression were quantified, and the densitometric values were normalized with the β-actin antibody, used as an internal loading control (Figure 4B).

ROS levels and antioxidant defences in *BCS1L* mutated fibroblasts.

To analyze the intracellular ROS levels, we first used confocal microscopy in control and mutant live cells incubated with DCF-DA, widely used to determine the intracellular levels of ROS, mainly oxygen peroxide (H_2O_2) (Figure 5A). Experiments showed increased H_2O_2 levels in patients P1, P2, P3 and P4 compared to controls, while these levels remained within control values in patients P5-P6. The H_2O_2 levels were next quantified by flow cytometry (Figure 5B), which confirmed a significant increase of H_2O_2 production in patients P1-P4, a not significant increase in patient P5, and normal H_2O_2 levels in patient P6.

Next, we analyzed the steady-state expression levels of the cellular antioxidant enzymes by Western-blot using whole cell lysates from control and *BCS1L* mutant fibroblasts (Figure 5C). The signals from triplicate blots were quantified by densitometry, normalized for the expression levels of β-actin, and then expressed as the percentage of control cells (Figure 5D). The steady-state levels of mitochondrial

manganese superoxide dismutase (MnSOD) were increased in patients P1, P3, P4 and P6, while patients P2 and P5 showed a normal expression of this enzyme. The catalase (CAT) steady-state levels were upregulated in patient P2, and downregulated in patient P3, while its expression was normal in the remaining patients. Another ROS scavenging enzyme, glutathione peroxidase (GPx), showed mildly increased steady-state levels in patients P1, P2 and P3, and a normal expression in the other patients. Finally, the glutathione reductase (GR) expression levels were only increased in patient P1. These results show a general overexpression of the antioxidant defences in all patients, except P5, compared to the controls.

Analysis of apoptotic cell death induction in *BCS1L* mutated fibroblasts.

Mitochondrial fragmentation and excessive ROS production have both been widely associated with programmed cell death (Suen et al., 2008; Valko et al., 2007). The possible effect of *BCS1L* mutations on cell death induction was evaluated by using an epifluorescence microscopy TUNEL assay (Figure 6A). Increased amounts of apoptotic nuclei were observed in fibroblasts from patients P1, P2 and P3, but unexpectedly, not in patient P4. Patients P5 and P6 also presented a similar number of apoptotic nuclei relative to the controls (Figure 6B). Accordingly, increased nuclear DNA fragmentation was confirmed in fibroblasts from patients P1, P2 and P3 (Figure 6C), suggesting an effect of their specific *BCS1L* mutations on cell death induction.

DISCUSSION

To better understand the pathophysiology of *BCS1L* mutations, we have characterized cultured skin fibroblasts from six complex III-deficient patients with defects in this putative complex III assembly factor. Based in our data, mutations in the *BCS1L* gene affect mitochondrial function at least at four levels: i) by altering the mitochondrial import and assembly of the BCS1L protein, thus hampering the biosynthetic pathway and activity of the BCS1L complex; ii) by destabilizing the RISP subunit; iii) by hindering the assembly or stability of respiratory complexes I, III and IV, which in turn would lead to increased ROS production and cell death; and iv) by inducing structural alterations in the mitochondrial network morphology.

Although no clear correlation could be established between the location of the mutations and the type of clinical presentation, the severity of the clinical phenotypes apparently correlated with the functional alterations observed in fibroblasts. In fact, in patients P1-P4, who consistently showed onset of symptoms at birth and early death, we found severe delays in cell growth rates, enzyme deficiencies and assembly defects of respiratory chain complexes I, III and IV, increased production of reactive oxygen species and altered expression of the ROS scavenging enzymes. Furthermore, cells from patients P1-P3 displayed a higher tendency to undergo apoptosis than controls and fibroblasts from the remainder patients. These alterations were evident in cells grown in glucose medium, in contrast with other studies in which the induction of metabolic stress was necessary in order to enhance the pathophysiological phenotypes of fibroblasts with OXPHOS defects (Guillery et al., 2008; Zanna et al., 2008). Although an initial limitation of this study was the fibroblast culture system, which uses a cell type that is probably less vulnerable to BCS1L defects than neurons and renal tubule cells that are affected in patients, our results highlight the severity of the respiratory chain dysfunction observed in these cells. Patients P5 and P6 presented relatively more

benign clinical courses, as evidenced by their later onset of symptoms and longer survival (i.e., they are still alive at ages 4-5 years). Accordingly, the fibroblasts from these patients displayed the best cell growth curves in glucose medium, mild or even normal enzyme activities and assembly of the mitochondrial respiratory chain complexes, normal ROS production, and they did not undergo apoptosis.

In control cells BCS1L is imported into mitochondria, where it possibly interacts with other proteins forming a ~400 kDa complex whose functional significance remains to be elucidated (Fernandez-Vizarra et al., 2009). In all patients´ fibroblasts, defects in the assembly or stability of the BCS1L complex were found in the form of accumulated low molecular weight subcomplexes that could be caused by structural alterations in the mutated BCS1L protein. Additionally, the assembly defects were partially due to a stalled import of the BCS1L protein, which would decrease the steady-state levels of the intramitochondrial BCS1L complex. Nearly all mutations were located at the N-terminal domain of BCS1L, which contains all the required information for the mitochondrial targeting and sorting of the protein (Folsch et al., 1996; Stan et al., 2003). This region holds a single transmembrane domain that is essential for anchoring the BCS1L protein into the inner membrane. The transmembrane domain is followed by an amphipathic α-helix that acts as an internal targeting signal. Immediately C-terminal there is an import-auxiliary region that, together with the amphipathic segment, is essential for the interaction with the TOM mitochondrial import machinery and the intramitochondrial sorting of BCS1L. The p.P99L mutation found in patient P1 probably modifies the tertiary structure of the BCS1L protein immediately after the mitochondrial auxiliary import domain (Folsch et al., 1996; Petruzzella et al., 1998; Stan et al., 2003). Patients P2 and P3 harboured the p.R56X nonsense mutation, which creates a premature stop codon in the membrane translocation domain, together with the p.R45C mutation, which changes a highly conserved aminoacid residue within the

amphipathic α-helix containing the internal targeting sequence (De Meirleir et al., 2003). Patient P4 also harboured the p.R56X nonsense mutation, plus the g.1181A>G and g.1164C>G mutations in the 5'UTR region of *BCS1L* mRNA that affected its stability (Gil-Borlado et al., 2009). By quantitative RT-PCR experiments, we previously demonstrated that out of the total amount of *BCS1L* transcripts expressed in the patient´s fibroblasts, ~15% of these harboured the p.R56X nonsense mutation, while the remainder transcripts (~85%) carried the 5'UTR mutations. The fact that the mRNA harbouring the p.R56X mutation was expressed at low levels suggested the expression of a truncated BCS1L protein. In this regard, the import-auxiliary region is partially lost in the 56-aminoacid BCS1L truncated form. In yeast, this region plays an essential role in the translocation of Bcs1p across the outer membrane, and a precursor lacking this region cannot be properly inserted into the inner membrane (Folsch et al., 1996). One possibility would be that in patients P2-P4, the BCS1L truncated form could compete with the BCS1L longer form, encoded by the second allele, for either its interaction with the TOM complex or its internalization into the inner mitochondrial membrane, impeding its proper import and intramitochondrial sorting. The p.T50A mutation found in patient P6 changes a mildly conserved aminoacid residue located at the beginning of the import auxiliary region (Blazquez et al., 2009) that also seems to affect the import of the BCS1L protein into the organelle. Interestingly, in patient P5 both the import and assembly of the BCS1L protein were mildly hampered, probably by effect of the p.R184C mutation, although the effect of a second unidentified mutation should also be considered. Studies in yeast Bcs1p support the importance of aminoacid residues close to the equivalent R184 position for Bcs1p activity and stability (Nouet et al., 2009).

In human cells, *BCS1L* knockdown caused the disassembly of the mitochondrial respiratory chain (Tamai et al., 2008). Accordingly, the steady-state levels of

mitochondrial complex III were severely decreased in our first three patients, who exhibited reduced expression levels of the complex III RISP subunit, and curiously, presented with iron overload. It might be possible that the RISP subunit that cannot be incorporated into complex III could undergo a rapid degradation. Another interesting possibility would be that BCS1L could be involved in the maturation of the Rieske subunit, i.e. through the incorporation of the iron sulphur cluster into the RISP protein. The observed reduction in complex III levels was accompanied by a mild decrease in the steady-state levels of respiratory chain complex I, probably as a result of the lack of stability of mitochondrial complex III (Acin-Perez et al., 2004). Moreover, decreased levels of mitochondrial complex IV were observed in two patients, suggesting a secondary role of BCS1L in complex IV maintenance. In agreement with this observation, other authors reported patients with *BCS1L* mutations who presented with combined deficiencies of respiratory chain complexes III and IV (Fernandez-Vizarra et al., 2007). Fibroblasts from patients P5 and P6, who showed either normal respiratory chain activities or a mild single complex III enzyme defect, respectively, exhibited normal assembly patterns of the respiratory chain complexes despite lower expression levels of the BCS1L complex. A similar observation was reported in Finnish patients with GRACILE Syndrome (Fellman et al., 2008).

Currently there are many unresolved questions concerning the intricate relationships between mitochondrial function and dynamics, ROS generation and apoptosis. In this regard, it has been previously proposed that the respiratory chain modulates apoptosis possibly through the generation of reactive oxygen species (Kwong et al., 2007), and that in this process the mitochondrial fusion and fission machineries are involved (Suen et al., 2008). Increased ROS production was previously shown in lymphoblasts from patients with *BCS1L* mutations associated with Björnstad Syndrome or complex III enzyme deficiency (Hinson et al., 2007). In our mutant cell lines, only

those mutations that affected more severely the mitochondrial respiratory chain function led to an overproduction of reactive oxygen species (patients P1-P4). Cells probably tried to compensate the increased accumulation of H_2O_2 by up regulating the expression of their antioxidant defences. However, the increased expression of the scavenging enzymes was probably not sufficient to compensate the high H_2O_2 levels in patients P1-P4. In fibroblasts from patient P5, the mutation was probably not causing an abnormal ROS generation because the respiratory chain enzyme activities were normal. Although cells from patient P6 exhibited a mild single complex III defect, suggesting some ROS generation through this complex, the high expression of the superoxide dismutase in this patient was probably sufficient to maintain ROS at normal levels. Our data thus support a direct link between defects in mitochondrial respiratory chain activities and ROS production, and agree with previous studies in which a direct correlation between the severity of OXPHOS defects and ROS production was observed (Verkaart et al., 2007). Conversely, in a recent work we showed normal ROS levels in fibroblasts from severely CI-deficient patients (Moran et al., 2010). These conflicting results may indicate that the impact on ROS production of mutations affecting OXPHOS complexes is not simple. Probably the effect of each mutation would depend on how it alters: i) the function/conformation of the affected protein, ii) the interactions with other respiratory chain components, and iii) as a result, the electron flux trough the whole respiratory chain. Therefore, not only the complex affected but also the type of mutation and the genetic background of each patient would play a role on mitochondrial ROS production. As expected, cells from patients P1-P3 displayed a higher tendency to undergo apoptosis than those from patients P4-P6. However, no clear correlation could be established between the rise in ROS levels and cell death, since in fibroblasts from patient P4, H_2O_2 was generated at high levels with no detectable cell death induction.

Earlier studies also suggested a role for BCS1L in the maintenance of mitochondrial morphology (Tamai et al., 2008). In support of these observations, all our *BCS1L* mutated fibroblasts presented fragmentation of the mitochondrial network, which could be partially amplified by the downregulated expression of the MFN2 protein. However, it is equally plausible that MFN2 is degraded because of the defect in mitochondrial function, thus further studies are necessary in order to elucidate this issue. Interestingly, these structural alterations neither correlated with the expression levels/defective activities of the mitochondrial respiratory chain complexes, nor with the increased ROS generation found in some cell lines. These data contrast with other studies where a clear correlation between the severity of respiratory chain complex I defects and a fragmented disposition of the mitochondrial network was documented (Koopman et al., 2005), and suggest that marked changes in mitochondrial morphology may occur independently from the mitochondrial respiratory chain function and ROS production.

Future functional studies based in the development of animal models, such as a conditional *BCS1L knock-out* mouse, not yet published, or a battery of *knock-in* mice harbouring different pathogenic mutations found in humans, will be of outmost importance to elucidate the precise mechanisms that interconnect these processes. These studies will probably allow to understand the different clinical manifestations of BCS1L-associated disorders, i.e., why the Björnstad Syndrome is so mild compared with GRACILE Syndrome or with complex III deficiency, or to demonstrate that the phenotypic variability of *BCS1L* mutations really depends on the nature of the mutation and the tissue-specific expression of the gene, a hypothesis that has been widely proposed (Hinson et al., 2007; Kotarsky et al., 2007; Ramos-Arroyo et al., 2009). This will contribute to a deeper understanding of mitochondrial diseases, and consequently, will improve the search of molecular targets to develop future therapeutic approaches.

ACKNOWLEDGEMENTS

We acknowledge Pilar del Hoyo for her excellent technical support. This work was supported by Instituto de Salud Carlos III (grant numbers PI05-0379 and PI08-0021 to C.U., and PI06-0547 to M.A.M.).

REFERENCES

Acin-Perez R, Bayona-Bafaluy MP, Fernandez-Silva P, Moreno-Loshuertos R, Perez-Martos A, Bruno C, Moraes CT, Enriquez JA. 2004. Respiratory complex III is required to maintain complex I in mammalian mitochondria. Mol Cell 13:805-815.

Baum H, Rieske JS, Silman HI, Lipton SH. 1967. On the Mechanism of Electron Transfer in Complex III of the Electron Transfer Chain. Proc Natl Acad Sci USA 57:798-805.

Benard G, Rossignol R. 2008. Ultrastructure of the mitochondrion and its bearing on function and bioenergetics. Antioxid Redox Signal 10:1313-1342.

Benit P, Lebon S, Rustin P. 2009. Respiratory-chain diseases related to complex III deficiency. Biochim Biophys Acta 1793:181-185.

Blazquez A, Gil-Borlado MC, Moran M, Verdu A, Cazorla-Calleja MR, Martin MA, Arenas J, Ugalde C. 2009. Infantile mitochondrial encephalomyopathy with unusual phenotype caused by a novel BCS1L mutation in an isolated complex III-deficient patient. Neuromuscul Disord 19:143-146.

Cruciat CM, Hell K, Folsch H, Neupert W, Stuart RA. 1999. Bcs1p, an AAA-family member, is a chaperone for the assembly of the cytochrome bc(1) complex. EMBO J 18:5226-5233.

de Lonlay P, Valnot I, Barrientos A, Gorbatyuk M, Tzagoloff A, Taanman JW, Benayoun E, Chretien D, Kadhom N, Lombes A, de Baulny HO, Niaudet P, Munnich A, Rustin P, Rötig A. 2001. A mutant mitochondrial respiratory chain assembly protein causes complex III deficiency in patients with tubulopathy, encephalopathy and liver failure. Nat Genet 29:57-60.

De Meirleir L, Seneca S, Damis E, Sepulchre B, Hoorens A, Gerlo E, Garcia Silva MT, Hernandez EM, Lissens W, Van Coster R. 2003. Clinical and diagnostic

characteristics of complex III deficiency due to mutations in the BCS1L gene. Am J Med Genet A 121A:126-131.

Fellman V. 2002. The GRACILE syndrome, a neonatal lethal metabolic disorder with iron overload. Blood Cells Mol Dis 29(3):444-50.

Fellman V, Lemmela S, Sajantila A, Pihko H, Jarvela I. 2008. Screening of BCS1L mutations in severe neonatal disorders suspicious for mitochondrial cause. J Hum Genet 53:554-558.

Fernandez-Vizarra E, Bugiani M, Goffrini P, Carrara F, Farina L, Procopio E, Donati A, Uziel G, Ferrero I, Zeviani M. 2007. Impaired complex III assembly associated with BCS1L gene mutations in isolated mitochondrial encephalopathy. Hum Mol Genet 16:1241-1252.

Fernandez-Vizarra E, Tiranti V, Zeviani M. 2009. Assembly of the oxidative phosphorylation system in humans: what we have learned by studying its defects. Biochim Biophys Acta 1793:200-211.

Folsch H, Guiard B, Neupert W, Stuart RA. 1996. Internal targeting signal of the BCS1 protein: a novel mechanism of import into mitochondria. Embo J 15(3):479-487.

Frickey T, Lupas AN. 2004. Phylogenetic analysis of AAA proteins. J Struct Biol 146:2-10.

Gil-Borlado MC, Gonzalez-Hoyuela M, Blazquez A, Garcia-Silva MT, Gabaldon T, Manzanares J, Vara J, Martin MA, Seneca S, Arenas J, Ugalde C. 2009. Pathogenic mutations in the 5' untranslated region of BCS1L mRNA in mitochondrial complex III deficiency. Mitochondrion 9:299-305.

Guillery O, Malka F, Frachon P, Milea D, Rojo M, Lombes A. 2008. Modulation of mitochondrial morphology by bioenergetics defects in primary human fibroblasts. Neuromuscul Disord 18:319-330.

Hinson JT, Fantin VR, Schonberger J, Breivik N, Siem G, McDonough B, Sharma P, Keogh I, Godinho R, Santos F, Esparza A, Nicolau Y, Selvaag E, Cohen BH, Hoppel CL, Tranebjaerg L, Eavey RD, Seidman JG, Seidman CE. 2007. Missense mutations in the BCS1L gene as a cause of the Bjornstad syndrome. N Engl J Med 356:809-819.

Iwata S, Lee JW, Okada K, Lee JK, Iwata M, Rasmussen B, Link TA, Ramaswamy S, Jap BK. 1998. Complete structure of the 11-subunit bovine mitochondrial cytochrome bc1 complex. Science 281:64-71.

Jiang D, Zhao L, Clapham DE. 2009. Genome-wide RNAi screen identifies Letm1 as a mitochondrial Ca2+/H+ antiporter. Science 326:144-147.

Koopman WJ, Visch HJ, Verkaart S, van den Heuvel LW, Smeitink JA, Willems PH. 2005. Mitochondrial network complexity and pathological decrease in complex I activity are tightly correlated in isolated human complex I deficiency. Am J Physiol Cell Physiol 289:C881-890.

Kotarsky H, Tabasum I, Mannisto S, Heikinheimo M, Hansson S, Fellman V. 2007. BCS1L is expressed in critical regions for neural development during ontogenesis in mice. Gene Expr Patterns 7:266-273.

Kwong JQ, Henning MS, Starkov AA, Manfredi G. 2007. The mitochondrial respiratory chain is a modulator of apoptosis. J Cell Biol 179:1163-1177.

Moran M, Rivera H, Sanchez-Arago M, Blazquez A, Merinero B, Ugalde C, Arenas J, Cuezva JM, Martin MA. 2010. Mitochondrial bioenergetics and dynamics interplay in complex I-deficient fibroblasts. Biochim Biophys Acta. doi: 10.1016/j.bbadis.2010.02.001.

Nijtmans LG, Henderson NS, Holt IJ. 2002. Blue Native electrophoresis to study mitochondrial and other protein complexes. Methods 26:327-334.

Nobrega FG, Nobrega MP, Tzagoloff A. 1992. BCS1, a novel gene required for the expression of functional Rieske iron-sulfur protein in Saccharomyces cerevisiae. EMBO J 11:3821-3829.

Nouet C, Truan G, Mathieu L, Dujardin G. 2009. Functional analysis of yeast bcs1 mutants highlights the role of Bcs1p-specific amino acids in the AAA domain. J Mol Biol 388:252-261.

Petruzzella V, Tiranti V, Fernandez P, Ianna P, Carrozzo R, Zeviani M. 1998. Identification and characterization of human cDNAs specific to BCS1, PET112, SCO1, COX15, and COX11, five genes involved in the formation and function of the mitochondrial respiratory chain. Genomics 54:494-504.

Ramos-Arroyo MA, Hualde J, Ayechu A, De Meirleir L, Seneca S, Nadal N, Briones P. 2009. Clinical and biochemical spectrum of mitochondrial complex III deficiency caused by mutations in the BCS1L gene. Clin Genet 75:585-587.

Santamaria G, Martinez-Diez M, Fabregat I, Cuezva JM. 2006. Efficient execution of cell death in non-glycolytic cells requires the generation of ROS controlled by the activity of mitochondrial H+-ATP synthase. Carcinogenesis 27:925-935.

Stan T, Brix J, Schneider-Mergener J, Pfanner N, Neupert W, Rapaport D. 2003. Mitochondrial protein import: recognition of internal import signals of BCS1 by the TOM complex. Mol Cell Biol 23:2239-2250.

Suen DF, Norris KL, Youle RJ. 2008. Mitochondrial dynamics and apoptosis. Genes Dev 22:1577-1590.

Tamai S, Iida H, Yokota S, Sayano T, Kiguchiya S, Ishihara N, Hayashi J, Mihara K, Oka T. 2008. Characterization of the mitochondrial protein LETM1, which maintains the mitochondrial tubular shapes and interacts with the AAA-ATPase BCS1L. J Cell Sci 121:2588-2600.

Valko M, Leibfritz D, Moncol J, Cronin MT, Mazur M, Telser J. 2007. Free radicals and antioxidants in normal physiological functions and human disease. Int J Biochem Cell Biol 39:44-84.

Verkaart S, Koopman WJ, van Emst-de Vries SE, Nijtmans LG, van den Heuvel LW, Smeitink JA, Willems PH. 2007. Superoxide production is inversely related to complex I activity in inherited complex I deficiency. Biochim Biophys Acta 1772:373-381.

Visapaa I, Fellman V, Vesa J, Dasvarma A, Hutton JL, Kumar V, Payne GS, Makarow M, Van Coster R, Taylor RW, Turnbull DM, Suomalainen A, Peltonen L. 2002. GRACILE syndrome, a lethal metabolic disorder with iron overload, is caused by a point mutation in BCS1L. Am J Hum Genet 71:863-876.

Xia D, Yu CA, Kim H, Xia JZ, Kachurin AM, Zhang L, Yu L, Deisenhofer J. 1997. Crystal structure of the cytochrome bc1 complex from bovine heart mitochondria. Science 277:60-66.

Zanna C, Ghelli A, Porcelli AM, Karbowski M, Youle RJ, Schimpf S, Wissinger B, Pinti M, Cossarizza A, Vidoni S, Valentino ML, Rugolo M, Carelli V. 2008. OPA1 mutations associated with dominant optic atrophy impair oxidative phosphorylation and mitochondrial fusion. Brain 131:352-367.

FIGURE LEGENDS

Figure 1. (A) Schematic representation of the *BCS1L* cDNA (NM_004328.4 Genbank reference sequence), slightly modified from (Fernandez-Vizarra et al., 2007). Aminoacid or nucleotide changes found in the patients (P1 to P6) are shown with arrows. Non-coding exons are indicated as -1 and -2. Coding exons representative of the BCS1L open-reading frame are indicated as 1 to 7. The numbered bar indicates the aminoacid position along the protein sequence. The ATG +1 translation initiation site is indicated in grey with an arrow. The BCS1L functional domains, deduced by homology with yeast bcs1, are indicated as follows: TMD, transmembrane domain; MTS, mitochondrial targeting sequence; IAS, import auxiliary sequence; BCS1L, activity and stability domain; AAA-ATPase, AAA-protein family specific ATPase domain. (B) Effect of the *BCS1L* mutations on cell growth. Cells were plated on P10 plates at $5x10^5$ cells per plate in glucose-containing media, and counted on a daily basis for 4 days. Each data point represents the mean ± SD of values obtained from each cell line tested at least in triplicate. C1-C2, control fibroblasts. P1-P6, patients' fibroblasts.

Figure 2. (A) Western-blot analysis of the BCS1L protein and mitochondrial respiratory chain subunits. Samples corresponding to 30 μg protein from whole fibroblast lysates were run through 10% SDS–PAGE gels and subsequently blotted. The levels of the BCS1L protein and the different respiratory chain subunits were detected using antibodies against the indicated proteins. The signal corresponding to β-actin was used for normalization. (B) Subcellular fractionations were performed in control and patients´ fibroblasts, and 15 μg protein from cytosolic fractions were subject to Western-blot analysis. (C) To evaluate the expression and assembly of the intramitochondrial BCS1L protein, BN-PAGE analysis was performed with mitochondrial-enriched fractions from control and *BCS1L* mutated fibroblasts, and

followed by Western-blot analysis using an antibody against BCS1L. The approximate molecular masses of three detected BCS1L complexes are indicated. (D) The assembly of the mitochondrial respiratory chain complexes was analyzed with 40 µg of digitonin-isolated mitochondria on 4-15% blue native gels. A complex I *in-gel* activity (IGA) assay is shown in the upper panel. Duplicate gels were subject to Western-blot analysis using antibodies against the following OXPHOS subunits: complex I (CI) NDUFS3, complex III (CIII) Rieske Iron-Sulfur protein (RISP), complex IV (CIV) subunit COX5A, and complex II (CII) SDHA subunit. C1-C3, controls. P1-P6, patients.

Figure 3. Mitochondrial morphology in control and *BCS1L* mutated fibroblasts grown in normal glucose media. (A) The mitochondrial morphology of fixed cells was analyzed by immunofluorescence using an anti-complex V α subunit antibody. C1-C2, controls. P1-P6, *BCS1L* mutated fibroblasts. Scale bar = 20µm. (B) Different shapes of the mitochondrial network. (a, b) depict controls with the classic filamentous mitochondrial network. The most numerous shapes found in patients´ fibroblasts included dense entangled perinuclear mitochondrial networks (c, d), intermediate shapes with elongated and short mitochondrial tubules (e, f), circular structures (g), small tubules with short branches (h, i, j), vesicles (k), and long fragmented mitochondria (l). (C) The proportion of cells with essentially elongated filamentous mitochondria (% of elongated), with an intermediate mitochondrial morphology (% of intermediate), or with only punctuate mitochondria (% of punctuate) was determined. Data are presented as mean ± SD of the analysis of >400 cells from each patient and five controls. (D) Mitochondrial diameter in mutant fibroblasts grown in normal glucose medium. The results shown are the means ± SD of at least 200 determinations from each cell line. One-way ANOVA analysis: significant main effect ($P<0.001$) was found. Scheffé test *post hoc*: *($P<0.01$), significantly different from controls.

Figure 4. Effect of the *BCS1L* mutations on the expression of proteins involved in mitochondrial dynamics. (A) 30 μg of total protein from fibroblast lysates were run through 10% SDS–PAGE gels and immunoblotted using specific antibodies against the indicated proteins. C1-C2, controls. P1-P6, patients´ fibroblasts. (B) Relative MFN2 expression levels. The signals from four independent blots were quantified, and normalized for the signal corresponding to β-actin. Data are presented as mean ± SD of the analysis of individual patients´ fibroblasts and 5 different controls (indicated as C). (a.u.), arbitrary units.

Figure 5. Increased ROS production and altered expression of the cellular antioxidant defences in the *BCS1L* mutated fibroblasts. Hydrogen peroxide levels were analyzed in live cells (A) by confocal microscopy, or (B) by flow cytometry, using DCF-DA as a probe. C-, control without DCF-DA incubation. C, control incubated with DCF-DA. P1-P6, patients´ fibroblasts incubated with DCF-DA. (C) Unbalanced expression of the cellular antioxidant defences. 30 μg of total protein from cell lysates were run through 10% SDS–PAGE gels and immunoblotted using the indicated antibodies. MnSOD, mitochondrial superoxide dismutase. CAT, catalase. GPx, gluthatione peroxidase. GR, gluthatione reductase. C1, C2, controls. P1-P6, patients. (D) The signals from three independent blots were quantified, and the densitometric values normalized with the anti-β-actin antibody. (a.u.), arbitrary units. Data are presented as mean ± SD of the analysis of individual patients´ fibroblasts and 5 different controls.

Figure 6. Effect of the *BCS1L* mutations on cell death. (A) Increased apoptotic cell death was observed in fibroblasts from patients P1, P2, and P3 by epifluorescence microscopy TUNEL assay. C, control. C+, positive control after 5 min incubation with 12,5 μg/ml DNAse I. (B) Apoptotic nuclei were quantified and the data are expressed as

the mean ± SD of the analysis of ~500 cells from each patient and 5 different controls.

(C) The relative DNA fragmentation was quantified using the Cell Death Detection ELISA^{PLUS} assay (Roche).

	P1	P2	P3	P4	P5	P6
Sex	Female	Male	Female	Male	Female	Male
Age at onset	Birth	Birth	Birth	Birth	19 months	6 months
Age at death	7 months	3 months	3 weeks	11 months	Alive (5 years)	Alive (4 years)
Fetal growth retardation	+	+	+	-	-	+
Lactic acidosis	+	+	+	+	+	+
Tubulopathy	+	+	-	+	-	-
Hepatopathy	+	+	+	+	+	+
Hypoglycemia	-	+	+	+	-	+
Failure to thrive	+	+	-	+	+	+
Encephalopathy	-	+	-	-	+	-
Hypotonia	+	+	+	+	-	+
Seizures	+	-	-	-	+	-
Microcephaly	+	-	-	+	-	+
Other symptoms		Ptosis		Anemia	Spasticity in the upper and lower limbs	Abnormal subcutaneous fat distribution, hypertrichosis, dysmorphic features, mild sensorineural hearing loss
Brain MRI	n.d.	Delayed myelination	Normal	Normal	Symmetric bilateral white matter lesions, bilateral hyperintense signals in thalamus	Normal
Laboratory data						
Iron overload	yes	yes	yes	no	n.d.	no
% CI Activity	n.d.	Normal	n.d.	n.d.	Normal	Normal
% CIII Activity	n.d.	**64%**	**39%***	**30%**	**38%**	**26%**
% CIV Activity	n.d.	Normal	Normal*	Normal	Normal	Normal
BCS1L mutations	**[p.P99L]+ [p.P99L]**	**[p.R56X]+[p.R45C]**	**[p.R56X]+[p.R45C]**	**[p.R56X] + [g.1181A>G, g.1164C>G]**	**[p.R184C]+[?]**	**[p.T50A]+[p.T50A]**

Table 1. Clinical, biochemical and genetic features of the *BCS1L*-mutated patients. Respiratory chain enzyme activities (in muscle homogenates, except *in fibroblasts) are expressed as the percentages of the residual enzyme activities relative to mean control values. CI, complex I. CIII, complex III. CIV, complex IV. n.d., not determined.

Table 2. Residual activities of the mitochondrial respiratory chain enzymes in cultured skin fibroblasts derived from controls and the index patients.

	Complex I	Complex II	Complex III	Complex IV	CS
Controls range (n=11)	26-50	10-18	28-87	52-105	60-160
Controls mean±SD	37±10	14±3	60±27	85±26	125±44
P1	**21.4**	16.4	**17.5**	**50.7**	85
P2	**24.0**	16.7	**17.8**	62.2	103
P3	n.d.	n.d.	n.d.	n.d.	n.d.
P4	29.4	**9.3**	**18.5**	**44.1**	65
P5	30.0	11.7	36.2	76.1	101
P6	27.1	11.2	**27.1**	59.5	105

Enzyme activities measured in our laboratory are expressed as nmol·min^{-1}·mg^{-1} protein. Abnormal values are indicated in bold characters. Enzyme activities of fibroblasts from patient P3 were previously measured in (De Meirleir, et al., 2003), and are indicated in Table 1. CS, citrate synthase. n.d., not determined.

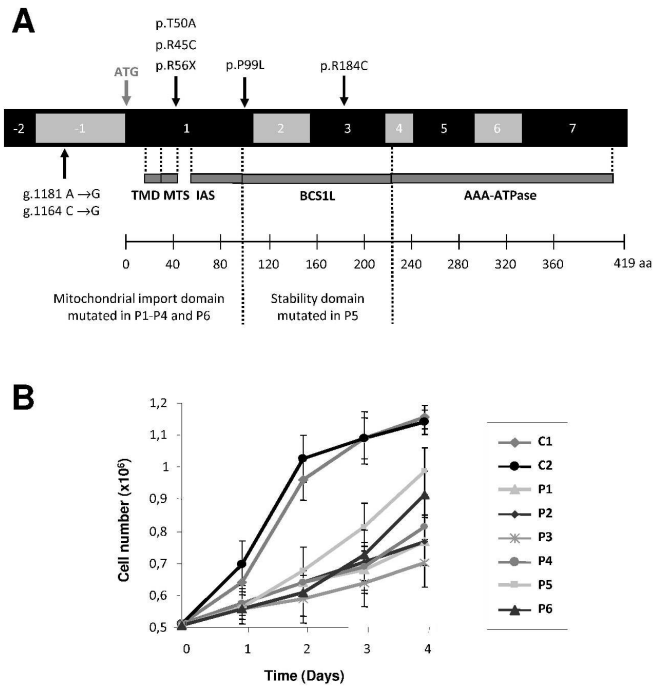

Figure 1

209x297mm (600 x 600 DPI)

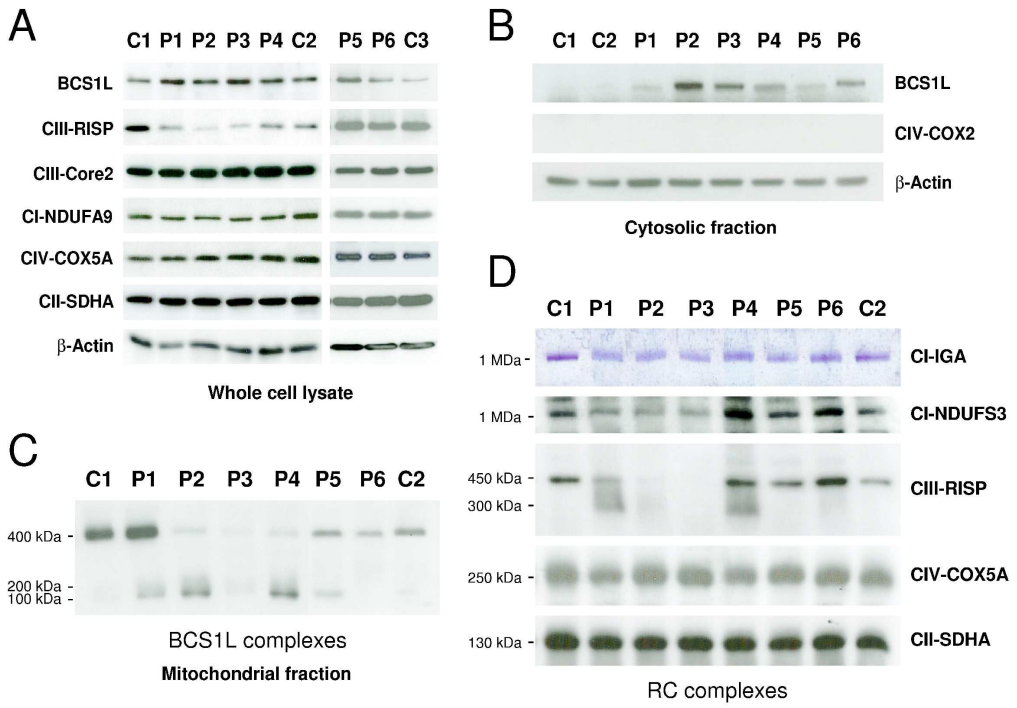

Figure 2

195x230mm (600 x 600 DPI)

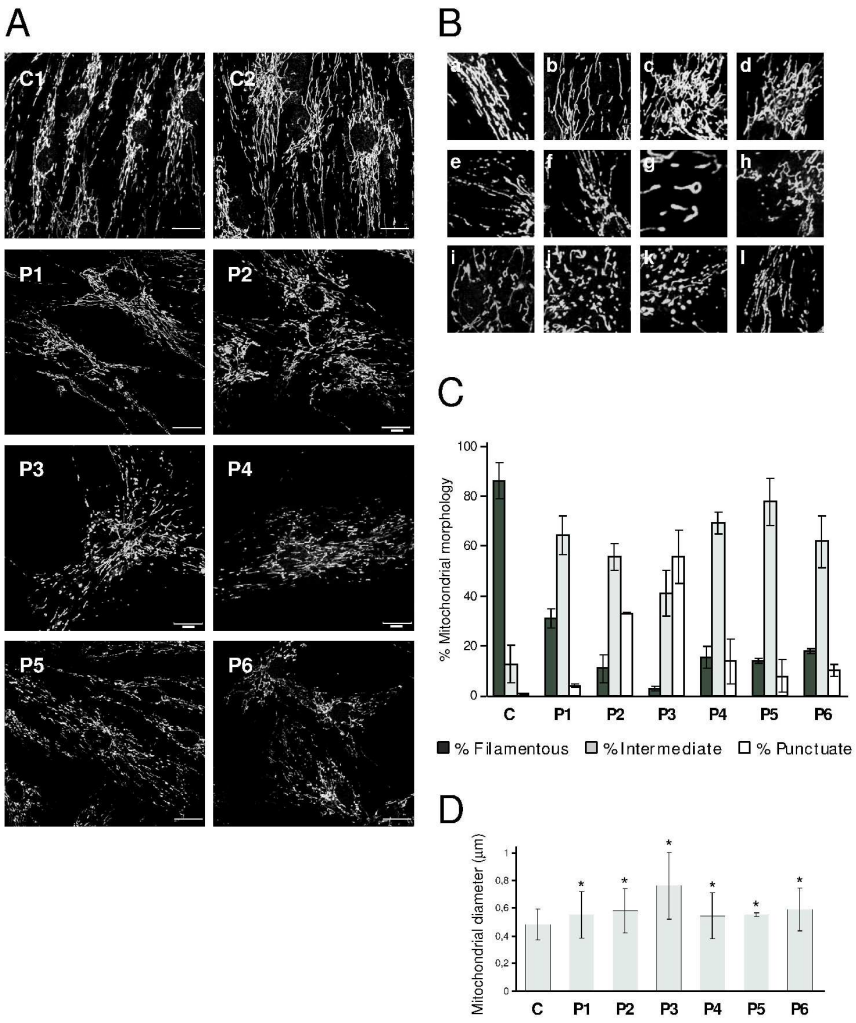

Figure 3

189x262mm (600 x 600 DPI)

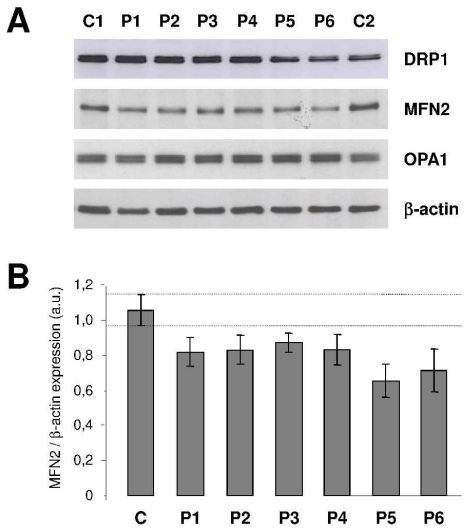

Figure 4

209x297mm (600 x 600 DPI)

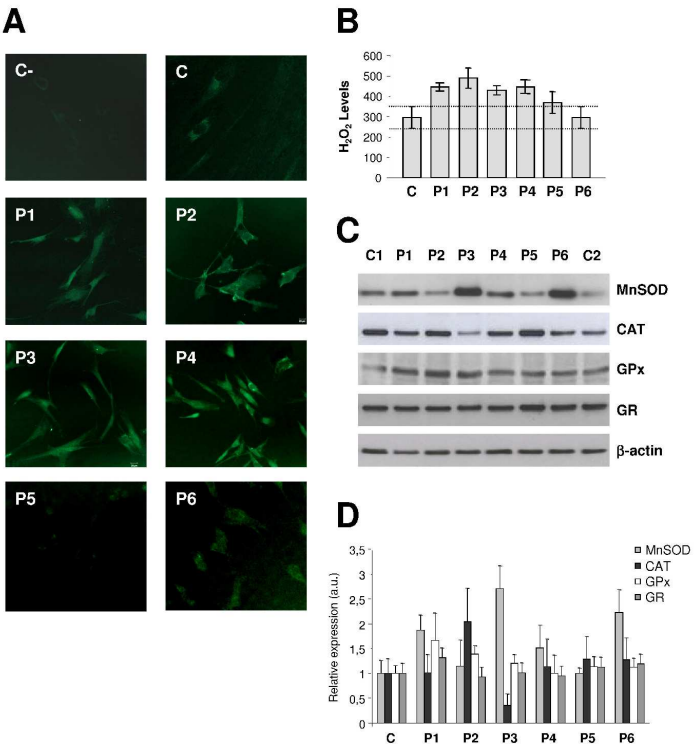

Figure 5

209x297mm (600 x 600 DPI)

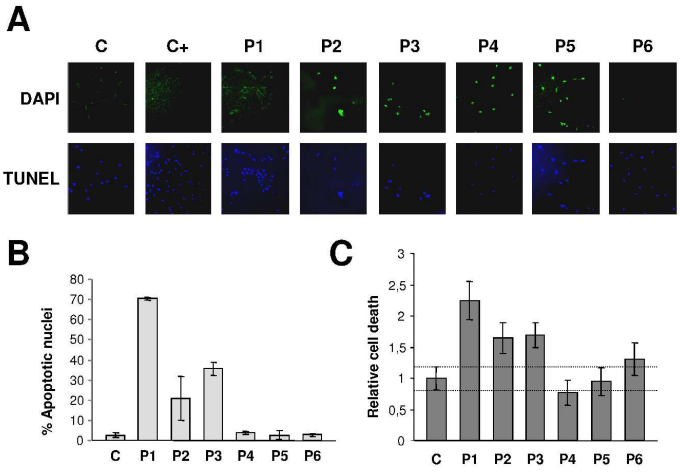

Figure 6

209x297mm (600 x 600 DPI)

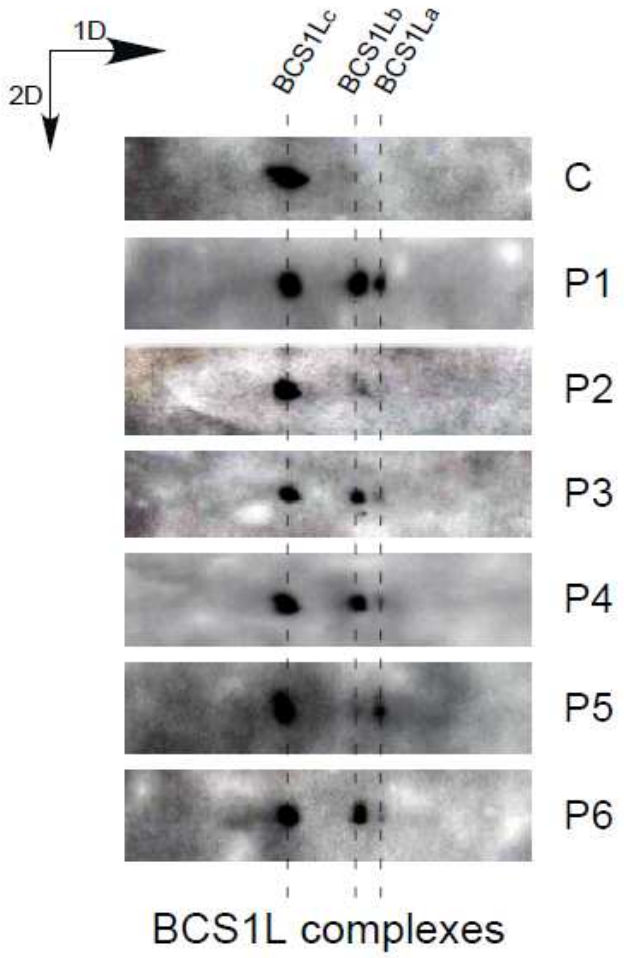

Supplemental Figure S1. For the separation of the individual components from the native BCS1L complexes, 10% tricine SDS-gels were run in the second dimension, blotted and incubated with the BCS1L antibody. The ~100 kDa and ~200 kDa subcomplexes that accumulate in the patients are indicated as BCS1La and BCS1Lb, respectively. BCS1Lc corresponds to the fully-assembled BCS1L complex. Arrows indicate the directions of the first (1D) and second (2D) dimensions, respectively.

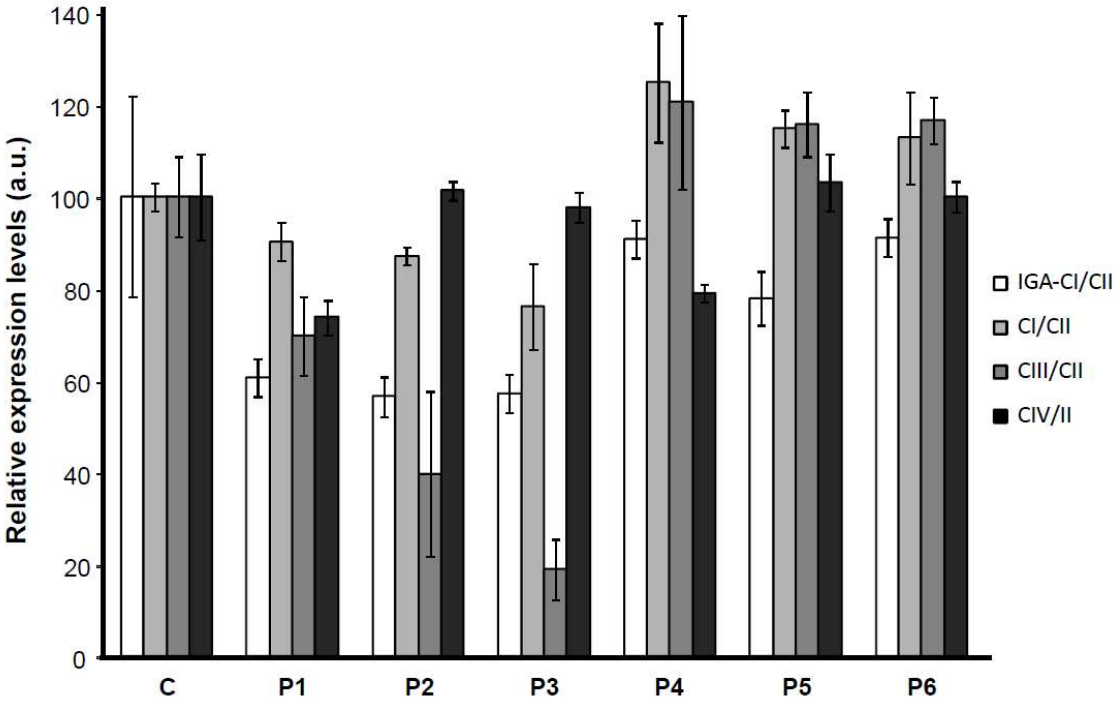

Supplemental Figure S2. The signals obtained from the IGA assays and Western-blots corresponding to the respiratory chain complexes from three independent blue native blots were quantified, the densitometric values were normalized for the expression levels of mitochondrial complex II, and expressed as the percentage of the control values. (a.u.), arbitrary units. Data are presented as mean ± SD of the analysis of individual patients´ fibroblasts (P1-P6) and 2 different controls (C).